ELSEVIER

Thin-Walled Structures 38 (2000) 105–123

THIN-WALLED STRUCTURES

www.elsevier.com/locate/tws

Simulations and experiments on active vibration control of a plate with integrated piezoceramics

Y. St-Amant, L. Cheng *

Laboratory of Vibro-Acoustics (LAVA), Department of Mechanical Engineering, Laval University, Québec, Canada G1K 7P4

Received 10 April 2000; received in revised form 9 June 2000; accepted 19 June 2000

Abstract

A frequency domain model on the basis of a rectangular plate with symmetrically integrated piezo-elements is extended to time domain suitable to use for on-line active vibration control simulations. Electromechanical effects of piezoceramic elements such as mass, stiffness and actuation are included in the model. The model is coupled to a control simulator comprising both Feedforward and Feedback algorithms. Simulations are made using the model to investigate some important aspects that may be encountered in practice such as system identification and control performance for different configurations. Finally, both controllers are implemented in DSP boards and experiments are carried out. Results demonstrate the representativeness of the system model and the efficiency of the algorithms for a SISO system. It is noted that the model developed in this paper is accurate and flexible enough to represent the real system in a control situation. The whole on-line simulation process is capable of reproducing reliable results to guide implementation of controllers. © 2000 Published by Elsevier Science Ltd.

Keywords: Vibration; Control; Active; Simulation; Experiment; Piezoceramic; Plate; Time; Domain; Model

1. Introduction

Active control using piezoceramic sensors and actuators has attracted attention of many researchers within the past decade. Successful implementation of active adapt-

* Corresponding author. Present address: Department of Mechanical Engineering, The Hong Kong Polytechnic University, Hong Kong.

E-mail address: mmlcheng@polyu.edu.hk (L. Cheng).

0263-8231/00/$ - see front matter © 2000 Published by Elsevier Science Ltd.
PII: S0263-8231(00)00034-3

ive controllers is usually based on the full understanding of the physical system, which significantly affects the control strategy, parameter tunings and convergence. This process proved to be tedious and difficult if it is done only by experiments. In this case, suitable simulation models are necessary to facilitate the development.

Efforts have been made during the last few years to develop suitable simulation models permitting easy parameter analyses to facilitate the design of such systems. One can find in the literature static models [1–3] in which the mass and the stiffness effects of the piezo-elements were neglected. Numerical models considering the full coupling between the piezo-elements and the host structures have also been developed [4,5]. Mostly, these models were developed to predict dynamic properties of the system in the frequency domain. By calculating the transfer functions between sensors and actuators, a lot of useful information can be obtained concerning the system dynamics, which can be indirectly used for the controller design. However, such models can hardly be used in real time control simulation, for which a time domain model would be more appropriate.

In our past work [6], a frequency domain model was developed on the basis of a rectangular plate with symmetrically integrated piezo-elements. Electromechanical effects of piezoceramics elements such as mass, stiffness and actuation were included in the model. In the present paper, the model is extended to the time domain, suitable to use for on-line active vibration control simulations. The model is firstly validated using experimental data. It is then coupled to a control simulator comprising both Feedforward and Feedback algorithms. Simulations were made using the model to investigate some important aspects involved in the control process such as system identification and control performance for different configurations. Finally, experimental studies using DSP boards are performed. Experimental results demonstrate the effectiveness of both the system model and the control algorithms.

It should be noted that the purpose of this paper is not to provide new control algorithms; rather, it is to illustrate how the developed model could help the design process before the implementation of controllers. In a general perspective, the work presented in this paper is one of the first steps in a long-term project on the active vibration control of airplane floor panels supported by Bombardier Aerospace in Toronto. One case, which is of particular interest and on which emphasis is put in this paper, is the vibration due to the multi-harmonic disturbances corresponding to the propeller blade passage frequencies.

2. Summary of the modeling procedure

This section briefly summarises the modelling procedure. Since part of the development is identical to the frequency domain model, only a minimum is given hereafter to ensure a good understanding of the methodology used. More details can be found in Ref. [6]. The part related to time domain simulation is presented in more detail.

The basic system consists of a thin rectangular plate, on which multiple piezoelectric elements are perfectly bonded symmetrically on each side as illustrated in

Fig. 1. The piezoelectric elements are used either as sensors or actuators. The boundary conditions of the plate are simulated by introducing a set of uniformly distributed virtual springs along each edge of the plate. A proper combination of the spring stiffness makes it possible to simulate all classical boundary conditions. The plate can be excited either by a point force or a control voltage on an actuator pair.

Kirchhoff–Love assumptions are used to build the displacement field for the whole system. The displacement field for the whole system is written as:

$$\{u,v,w\}=\left\{-z\frac{\partial w}{\partial x},-z\frac{\partial w}{\partial y},w(x,y,t)\right\} \tag{1}$$

where the vector $\{u, v, w\}$ represents the displacement of a point either on the plate or on the piezoceramic elements. Perfect bonding is considered between the plate and piezoelectric elements.

Rayleigh–Ritz approximations are used to solve the system with the following polynomial series expansion over x and y:

$$w(x,y,t)=\sum_{i=0}^{m}\sum_{j=0}^{n}a_{ij}(t)\left(\frac{x}{b}\right)^{i}\left(\frac{y}{h}\right)^{j} \tag{2}$$

where $a_{ij}(t)$ are the complex and time-dependant variables to be determined.

The analytical formulation is based on the variational approach, in which the energy of the whole system is extremalized by means of the Lagrange equations. Using the coefficient $a_{ij}(t)$ as the generalized coordinates, Lagrange equations can be written in the following general form:

$$\frac{\mathrm{d}}{\mathrm{d}t}\left(\frac{\partial L}{\partial \dot{a}_{\mathrm{pq}}}\right)-\frac{\partial L}{\partial a_{\mathrm{pq}}}=0 \quad (p=0,1,2,\ldots,m \text{ and } q=0,1,2,\ldots,n) \tag{3}$$

where L is the Lagrangian of the system expressed as:

$$L=E_{\mathrm{kin}}-E_{\mathrm{p}}+W \tag{4}$$

where E_{kin} represents the total kinetic energy of the system, E_{p} the total potential energy of the system and W the work done by the external forces. Details on the

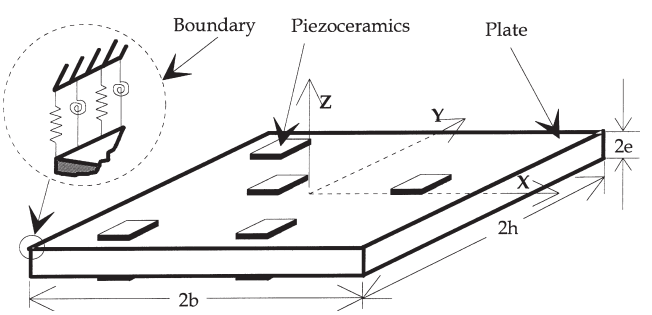

Fig. 1. Plate configuration.

terms related to the plate, the boundaries and the work done by the external forces can be found in [6].

The total enthalpy density (H) of a piezoelectric element [7] is used to find the energy expression of the piezoceramic elements by considering only the transverse electric field E_3:

$$H=0.5[T_{11}S_{11}+T_{22}S_{22}+2T_{12}S_{12}]-[e_{31}E_3(S_{11}+S_{22})]-[0.5\varepsilon_{33}E_3^2] \tag{5}$$

where ε_{33} is the permitivity; T_{ij} the stress; S_{ij} the strain and e_{31} the piezoelectric constant. The stress term T_{ij} and the strain term S_{ij} can be easily expressed in terms of the displacement of the plate using Eq. (1). The energy expression of each piezoceramic element can be found by integrating Eq. (5) over its own volume.

For actuator, after minimization, the first term in Eq. (5) represents the rigidity of the piezoelectric elements, the second one, the energy supplied by the actuator to the structure, and the last term disappears. Eq. (5) is also applicable for a sensor. Being passive element, however, only the first term of Eq. (5) is retained representing its rigidity.

Using Lagrange Eq. (3) with Eq. (2) leads to the following system of differential equations:

$$\mathbf{M}\ddot{\mathbf{A}}(t)+\mathbf{K}\mathbf{A}(t)=\mathbf{F}(t)+\mathbf{Q}(t) \tag{6}$$

where $\mathbf{M}$ and $\mathbf{K}$ are respectively the mass and the stiffness matrix of the system. $\mathbf{F}(t)$ is the external generalized force vector and $\mathbf{Q}(t)$, the generalized excitation vector provided by actuators. $\mathbf{A}(t)$ is the generalized coordinate vector to be determined.

In our past work [6], a structural damping was introduced in the system which was only valid for harmonic excitations. In this work, arbitrary excitations are investigated, which implies the necessity of using a new damping definition. Proportional damping has been chosen for this purpose. Proportional damping assumes that the damping matrix is proportional to the mass and stiffness matrix. Let $\mathbf{R}$ be the modal matrix which is the eigenvector of the system $\{X^i\}$:

$$\mathbf{R}=\text{eigenvector}(\mathbf{M}^{-1}\mathbf{K})=[\{X\}^1\ldots\{X\}^N] \tag{7}$$

By decoupling the matrix system (6), the following damping matrix of the system $\mathbf{C}$ is defined:

$$\mathbf{C}=\mathbf{M}\mathbf{R}\begin{bmatrix} 2\zeta_1\omega_1 & 0 & \cdots & 0 \\ 0 & \ddots & & \vdots \\ \vdots & & \ddots & 0 \\ 0 & \cdots & 0 & 2\zeta_N\omega_N \end{bmatrix}\mathbf{R}^{-1} \tag{8}$$

where ζ_i and ω_i are respectively the modal damping factors and the natural frequencies of the system. By introducing this term in the general equation of the system (6), we can obtain the following differential equations of the damped system:

$$\mathbf{M}\ddot{\mathbf{A}}(t)+\mathbf{C}\dot{\mathbf{A}}(t)+\mathbf{K}\mathbf{A}(t)=\mathbf{F}(t)+\mathbf{Q}(t) \tag{9}$$

The above equation should be resolved upon imposing the initial conditions. Details will be given in the following section. Finally, the sensor output voltage is calculated using the capacitance C of each sensor and the electric charge $q(t)$ which can be obtained from the dielectric displacement:

$$V_s(t)=\frac{q(t)}{C} \tag{10}$$

3. Time domain resolution and validations

To resolve the system (9), Newmark method was used [8]. With this implicit method, the position vector $\mathbf{A}$ at time $t+\Delta t$ is found with the position vector $\mathbf{A}$, the velocity vector $\dot{\mathbf{A}}$ and the acceleration vector $\ddot{\mathbf{A}}$ at time t. The algorithm used is briefly summarised as follow.

Considering Eq. (9) and replacing the sum of generalized force vectors by $\mathbf{S}(t)$,

$$\mathbf{M}\ddot{\mathbf{A}}(t)+\mathbf{C}\dot{\mathbf{A}}(t)+\mathbf{K}\mathbf{A}(t)=\mathbf{S}(t) \tag{11}$$

and knowing the initial position and velocity conditions

$$\dot{\mathbf{A}}(t)_{t=0}=\{\dot{A}(0)\},\ \mathbf{A}(t)_{t=0}=\{\mathbf{A}(0)\} \tag{12}$$

Find the initial acceleration vector of the system:

$$\ddot{\mathbf{A}}(t)_{t=0}=\{\ddot{A}(0)\}=\mathbf{M}^{-1}(\mathbf{S}_{t=0}-\mathbf{C}\dot{\mathbf{A}}(t)_{t=0}-\mathbf{K}\mathbf{A}(t)_{t=0}) \tag{13}$$

Compute the residual expression:

$$\hat{\mathbf{K}}=\mathbf{M}+\Delta t\, a\mathbf{C}+\frac{(\Delta t)^2}{2}b\mathbf{K} \tag{14}$$

where a and b are chosen to be 1/2 et 1/3 respectively, which suppose that the acceleration is varying linearly over Δt.

The position, velocity and acceleration vectors at time t becomes respectively:

$$\mathbf{A}(t+\Delta t)=\hat{\mathbf{K}}^{-1}\mathbf{R}(t+\Delta t) \tag{15}$$

where

$$\mathbf{R}(t+\Delta t)=\frac{(\Delta t)^2}{2}b\mathbf{S}(t+\Delta t)+\mathbf{M}\left(\mathbf{A}(t)+\Delta t\dot{\mathbf{A}}(t)+\frac{(\Delta t)^2}{2}(1-b)\mathbf{A}(t)\right) \tag{16}$$

$$+\mathbf{C}\left(\Delta t a\mathbf{A}(t)+\frac{(\Delta t)^2}{2}(2a-b)\dot{\mathbf{A}}(t)+\frac{(\Delta t)^3}{2}(a-b)\ddot{\mathbf{A}}(t)\right)$$

$$\ddot{\mathbf{A}}(t+\Delta t)=\frac{1}{b}\left((\mathbf{A}(t+\Delta t)-\mathbf{A}(t)-\Delta t\dot{\mathbf{A}}(t))\frac{2}{\Delta t^2}-(1-b)\ddot{\mathbf{A}}(t)\right) \tag{17}$$

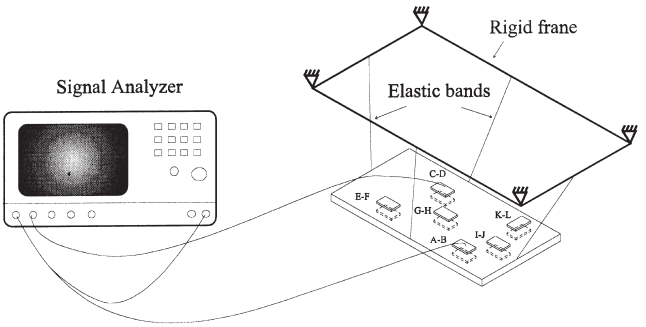

Fig. 2. Experimental set-up for validation.

$$\dot{\mathbf{A}}(t+\Delta t)=\dot{\mathbf{A}}(t)+\Delta t((1-a)\ddot{\mathbf{A}}(t)+a\ddot{\mathbf{A}}(t+\Delta t)) \tag{18}$$

This algorithm has been validated for several well-known discrete and continuous systems with various initial conditions.

The time domain model was validated using experimental data. Fig. 2 shows the experimental set-up used. To create free boundary conditions, the plate was attached to a rigid steel frame by four rubber bands with very weak stiffness. An actuator pair was used to excite the structure. Polytec PIC 141 piezoceramic elements were used for the validation. Six pairs of piezoelements were bonded to the plate surface at locations illustrated in Fig. 2. Characteristics of the plate and the piezoelements are summarised in Table 1 and locations of piezoelements are presented in Table 2. A white noise (0–1200 Hz) generated by a 2035 B & K analyzer was applied to the selected pair of PZTs (A–B) and a single piezoelement (C–D) was used to measure the plate response. For the simulation, a white noise generated at 20480 Hz was applied to the actuator (A–B). The sensor output (C–D) was then calculated. Fig. 3 presents the simulated time domain data for the actuator and the sensor.

Table 1
Dimensions and physical properties of materials

	Plate	Piezoelements Polytec PIC141
Width ($2b$) [mm]	260	30
Length ($2h$) [mm]	500	50
Thickness (2e)[mm]	2.26	0.4
Density (ρ)[kg/m^3]	2700	7800
Permitivity	–	– (Actuator) 0.1157E-7 (Sensor)
Young's modulus (E) [GPa]	70	79.365 (Actuator) 87.689 (Sensor)
Piezoelectric constant (e_{31})	–	9.127 (N/m.V)
Damping factor	0.005	–
Poisson ratio (v)	0.30	0.30

Table 2
Locations of piezoelements (mm)

A–B	C–D	E–F	G–H	I–J	K–L
(−65,−126)	(65,75.5)	(−65,125)	(0,−1)	(0,−175)	(89.5,−150)

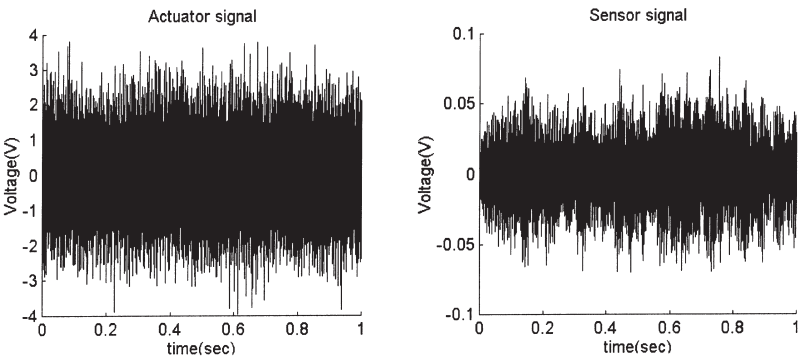

Fig. 3. Simulated time domain data.

Fourier transform is then performed on the time domain data to obtain the numerical transfer function between the actuator (A–B) and the sensor (C–D). A comparison between simulation and experimental transfer functions is presented in Fig. 4. The three curves (in dB referenced to 1) appearing in the figure correspond to the results of the time domain model, the frequency domain model and experimental measurements.

It can be seen that resonant peaks are well predicted by the simulation model, showing that the boundary conditions of the plate, the mass, stiffness and active

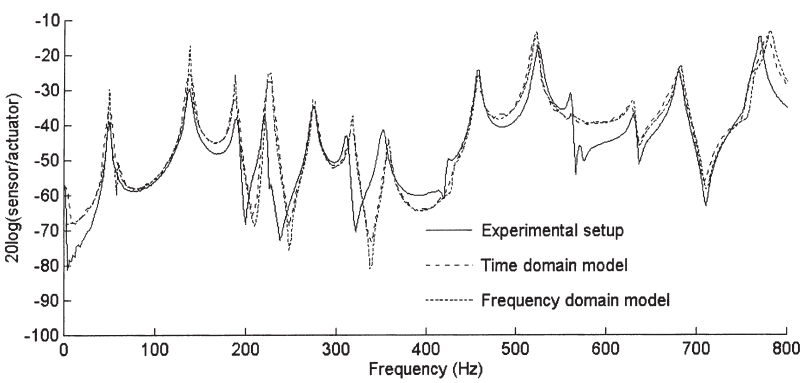

Fig. 4. Sensor–actuator transfer function: experimental data (———), time domain model data (- - -) and frequency domain model data (· · ·).

effects of the PZT are reasonably well simulated. The model is particularly accurate in the low and middle frequency ranges as well as in resonance regions. More obvious discrepancies can be observed in off-resonance regions and this state of affairs is slightly amplified with the increase in frequency. This difference may be attributed to the exclusion of the bounding layer in the simulation model, which certainly becomes more important to be taken into account at high frequencies. However the model seems to be accurate enough to predict the general dynamic tendency of the system for most active control simulation purposes. Very nice agreement exists between the time domain model and the frequency domain model.

When using the time domain model, special care is needed in order to produce reliable data. In fact, simulations should be performed using a sufficiently high sampling rate in order to cover the whole frequency range of interest. Typically, the sampling frequency should be approximately 20 times higher than the highest frequency considered.

We can conclude that the developed model is very representative of a physical system composed of a plate with multiple integrated piezoelements and it can be used to develop and test active control algorithms.

4. Control algorithms and control simulations

In this paper, two control algorithms are coupled with the previously developed model. The first one is a feedforward control algorithm with an adaptive FIR controller based on LMS algorithm [9], shown in Fig. 5. The feedforward control assumes that a reference signal related to the disturbance is available and that this signal is not affected by the secondary source. This reference signal is used to feed the controller. In this scheme, a FIR controller has been chosen for its stability. Having the control path placed in the output of the adaptive FIR filter, a copy of the transfer function is placed in the input of the LMS algorithm leading on the use of the FXLMS algorithm. The desired output is zero since we want to eliminate sensor response.

The second one is the feedback algorithm (also called feedforward control with internal model) with an adaptive FIR controller based on LMS algorithm as shown

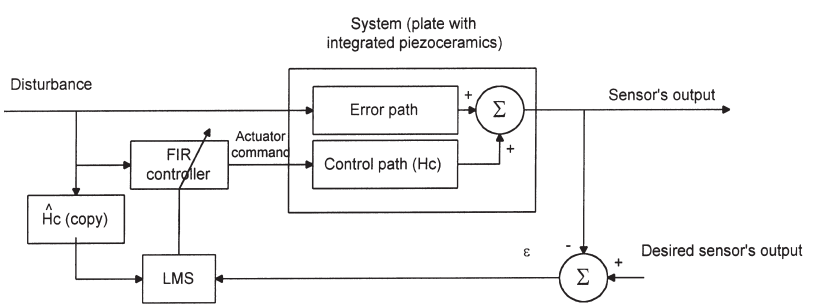

Fig. 5. Feedforward control with FIR controller.

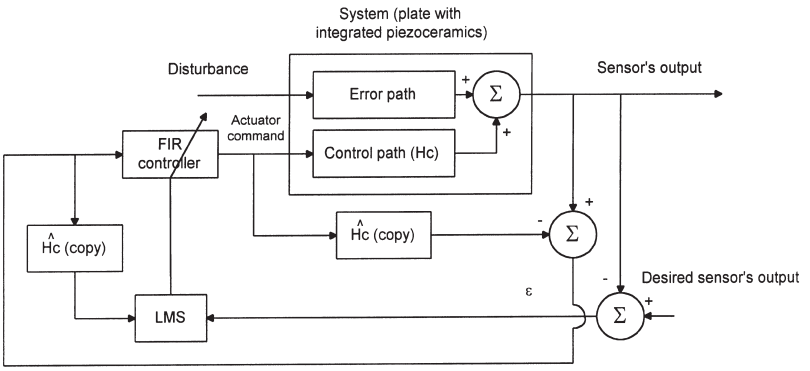

Fig. 6. Feedback Control with FIR controller.

in Fig. 6. In this case, no direct reference signal is, a priori, needed. A copy of the control path is used to find the sensor response due to the control path. By removing the participation of the control path in the sensor response, one can get an approximation of disturbance filtered by the error path. Then, we get something like a reference signal that we can provide to the FIR controller. This is the reason for which this algorithm can also be regarded as a feedforward control with internal model. Once again, because the control path is placed in the output of the FIR controller, the FXLMS algorithm should be used.

In both cases, the control path must be identified to generate a filtered-X signal as a reference input to the LMS algorithm. This is done by exciting the actuator with a white noise and measuring the response at the sensor. After data collection of the discrete transfer function of the control path, an ARX model is identified off-line using a least square approach, which leads to an Infinite Impulse Response (IIR) filter model.

The simulated system is shown in Fig. 7 where the vibration level at the sensor location is to be minimized by the action of an actuator pair. Note that one pair of PZT is used as actuator while the other one as sensor. This non-collocated configur-

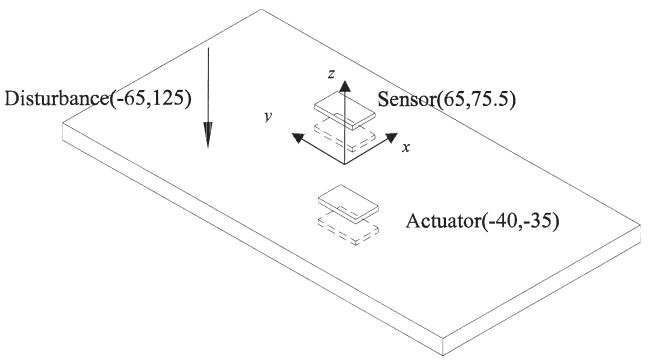

Fig. 7. Simulated system.

ation is believed to be more effective to generate the flexural motion of the plate. The disturbance used is a point mechanical force. Free boundary conditions are assumed for the plate. Table 1 shows properties of each element.

Control path identification. As explained in the previous section, an off-line identification of the control path is firstly archived. While a random signal with unit variance was applied to the actuators, the response voltage at the sensors was calculated using the simulator as shown in Fig. 8. In this figure, two sets of boxes are drawn. The dotted boxes represent the data used for the identification and the dashed ones represent the data used for validation purposes. An ARX model using 28 direct coefficients and 27 recursive coefficients is used to identify the control path with the identification data. A closer view of the validation box is given in Fig. 8(c) in

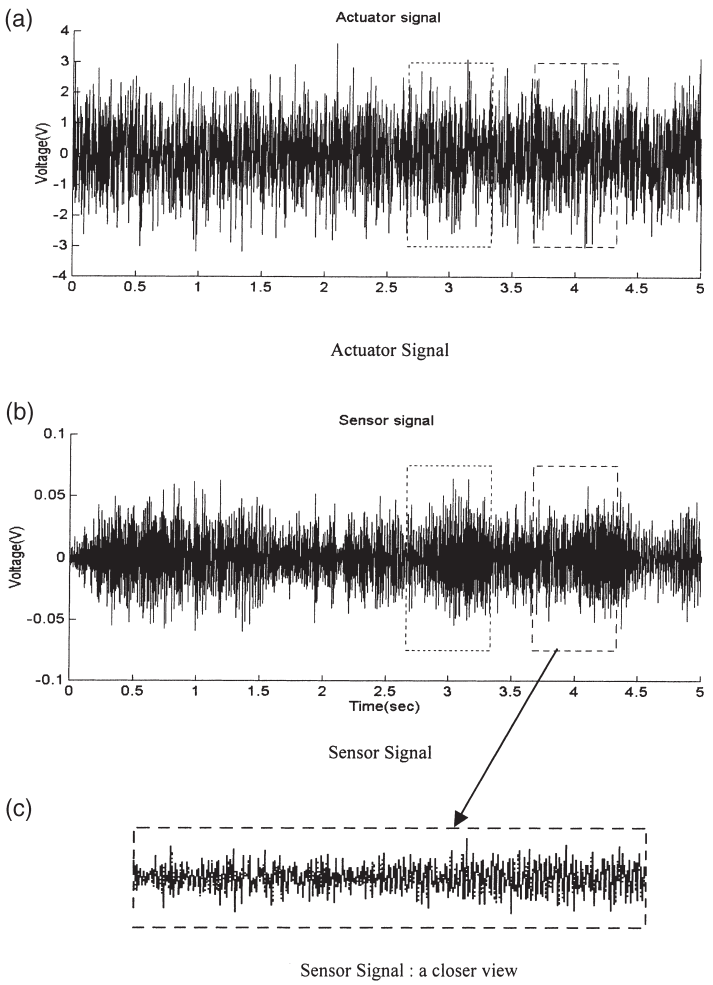

Fig. 8. (a) Simulated data used to identify and validate the control path model; (b) and (c) time domain validation: Numeric model (———) and ARX model (- - -) response.

which numerical data coincide well with the data predicted by ARX model. Fig. 9 compares the frequency response of the ARX model (- - -) and the one generated using simulation model (———). Good agreement can be noticed particularly below 250 Hz. It can be noticed that the content of frequency below 250 Hz including nine resonances is very well represented by the ARX model. It should be noted that the present configuration is different from the one used in Fig. 4 in terms of number and locations of the PZTs. Using only two PZTs in the present case, the plate is much less stiffened, leading to lower natural frequencies compared to Fig. 4.

Feedforward control. Using the Feedforward algorithm, two control cases corresponding to different disturbances are presented in the Fig. 10: a single frequency case and a typical situation involving a fundamental frequency and its harmonics, which is often encountered in an airplane vibration problems. In both cases, the sensor outputs were plotted in time domain. The controller is turned on after 3 s. A total duration of 10 s was simulated. It can be seen that, for both single frequency disturbance and multi-harmonics, the feedforward control can effectively attenuate the sensor output within a relatively short time. Comparing the mean absolute value (MAV) of the sensor signal with and without control, an attenuation of 35 dB after 7 s can be observed in the single frequency case and an attenuation of 38.5 dB in the multi-harmonic case.

Other test cases using Feedforward controller have also be performed. Simulation results are summarised in the left half of Table 3. Similar conclusions can be drawn.

Feedback control. Simulations on the same configurations were also performed using the Feedback control for comparison purposes. Fig. 11 shows the results. Again, it can be seen, for both a pure frequency and multi-harmonic disturbances, the feedback controller can effectively attenuate the sensor output within relatively short time. An attenuation of 42 dB after 4 s was obtained in single frequency case. For the multi-harmonic signal, an attenuation of 12 dB after 6 s was observed. Feedback control performances for different kinds of disturbance signal are summarised in Table 3. Comparing the performance of both controllers in multi-harmonic case,

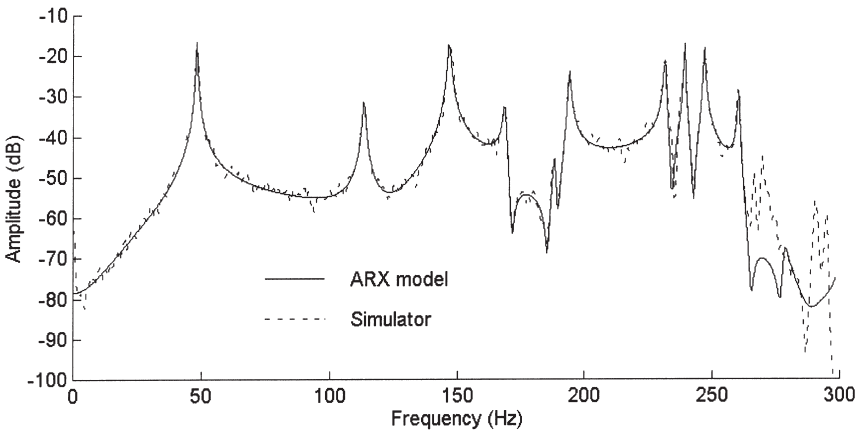

Fig. 9. Measured (———) and identified (- - -) frequency response.

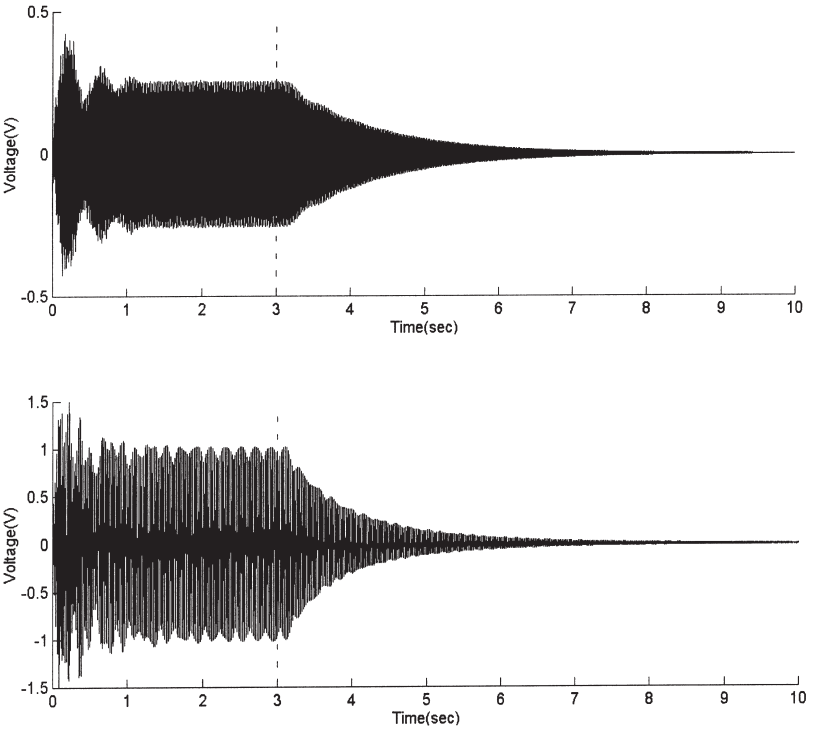

Fig. 10. Feedforward control of different disturbances: (a) a single frequency signal (49.5 Hz); (b) a multi-harmonic signal (55, 110 and 165 Hz).

Table 3
Control performance for active control simulation

Feedforward control			Feedback control		
Perturbation	Time (s)	Attenuation (dB)	Perturbation	Time (s)	Attenuation (dB)
Resonance (49.5 Hz)	7	35	Resonance (49.5 Hz)	4	42
Anti-resonance (122 Hz)	7	34	Anti-resonance (122 Hz)	3	44
Non-resonance (111 Hz)	7	45	Non-resonance (111 Hz)	3	34
Multi-harmonic case (55, 110 and 165 Hz)	7	38.5	Multi-harmonic case (55, 110 and 165Hz)	6	12

one notices that feedback controller is less effective. It should be noted that at the present stage no noise contamination was included in our simulations. The presence of the noise should in principal affect even more the performance of the feedback controller, which proved to be more sensitive to the feedback noise, as will be illustrated later by experimental tests.

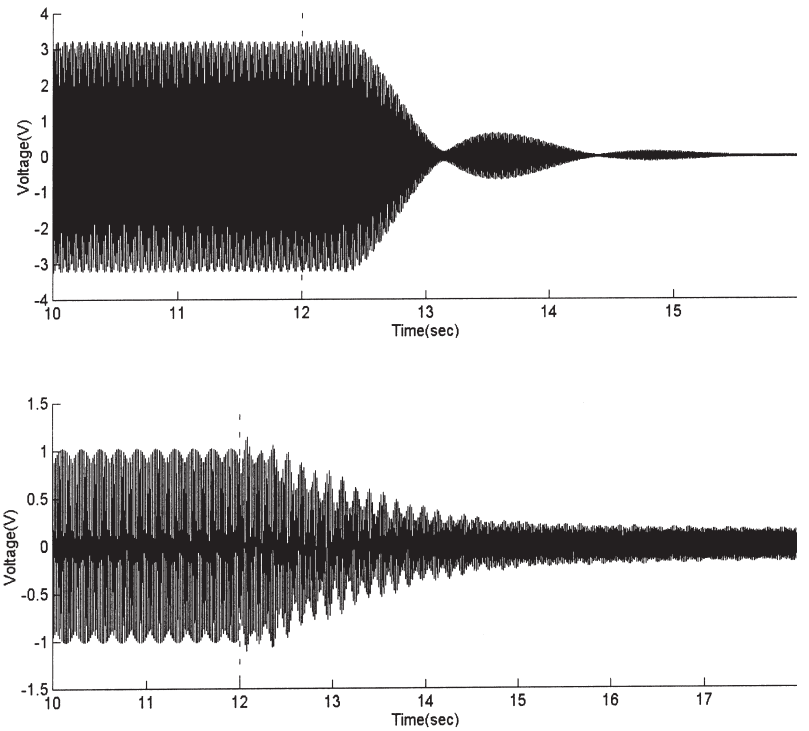

Fig. 11. Feedback control of different disturbances: (a) a single frequency signal (49.5Hz); (b) a multi-harmonic signal (55, 110 and 165 Hz).

5. Experimental implementations

On the basis of the simulation results presented in the previous section, an active vibration control system was developed for the active control of a real structure. Fig. 12 presents this closed-loop control system. The experimental set-up consists of four parts: plate, amplifiers, DSP controller and user-machine interface (hosted in a Pentium II 233 MHz PC with MATLAB).

Dimensions of the plate and locations of piezoelements are identical to those presented in Tables 1 and 2. Piezoelements E and F are used as error sensors, piezoelements G and H act as control actuators and piezoelements A and B act as an external disturbance. Those pairs of piezoelements will be respectively named sensor, actuator and disturbance in the following sections. Fig. 13 presents the DSP development environment. Functionality of the DSP controller includes a 4th Order Chebyshev anti-aliasing filter (340 Hz), A/D (14 bits) and D/A (16 bits) conversion, control law execution and communication with the computer. The aforementioned algorithms are implemented in a DSP based unit which is a product of the DIGISONIX Inc. using Texas Instrument TMS320C30 boards. The computer allows to change parameter configuration of the control system and to display results.

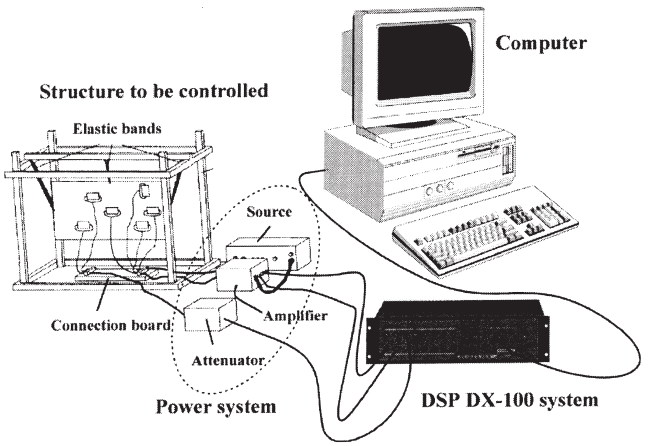

Fig. 12. Closed-loop vibration control experimental set-up.

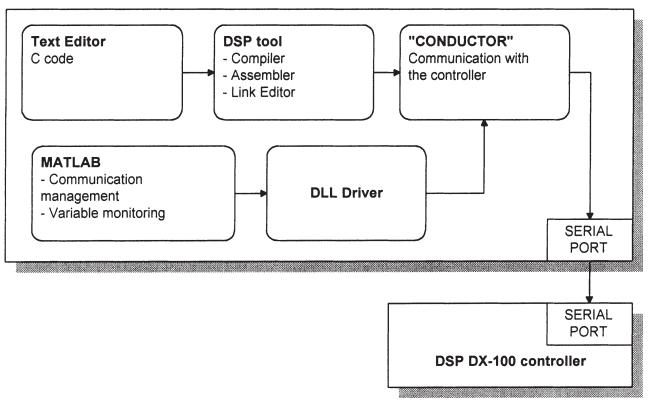

Fig. 13. DSP development environment.

Similar to simulations, an off-line identification of the control path between the actuator and the sensor is first performed. The generation of the white noise excitation and acquisition of the sensor output were conducted by means of the DSP controller with a sampling frequency of 1000 Hz as for the control situation. An ARX model using 27 direct coefficients and 26 recursive coefficients is used to identify the control path. Fig. 14(a) compares the frequency response of the ARX model and the measured one. Good agreement can be observed below 340 Hz. Fig. 14(b) presents the pole-zero plot of the ARX model showing the stability of the model.

Feedforward controller is first tested using two typical disturbances: single frequency and multi-harmonic disturbances. Results are respectively given in Figs. 15 and 16, in both time domain and frequency domain by performing a FFT using time data.

As predicted by simulations, the feedforward controller attenuates the sensor out-

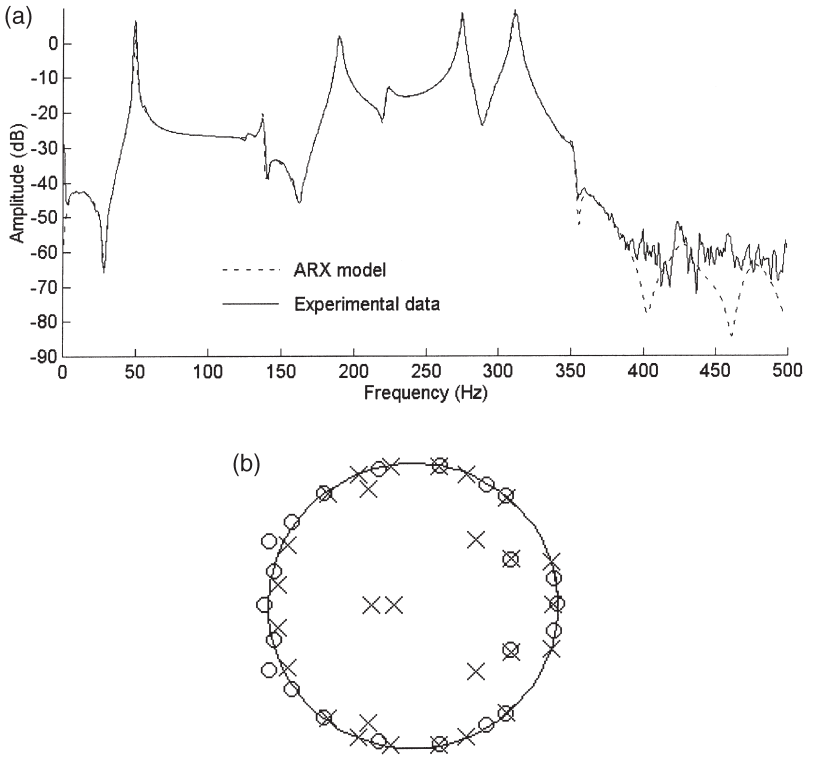

Fig. 14. (a) Measured (———) and identified (- - -) frequency response; (b) pole-zero plot of the ARX model (×=pole, ○=zero).

put within relatively short time. Comparing the MAV, an attenuation of 29.8 and 27.8 dB can be obtained for the single frequency disturbance and the multi-harmonic disturbance, after 6 and 7 s respectively. Results of other experimental tests are summarised in Table 4. An analysis of spectrums gives more details on the performance of the controller. In the single frequency case, Fig. 15(b) shows the slight nonlinearity of the system. In fact, harmonics of the 49.5 Hz components can be clearly seen. Although the controller is basically a linear one, it can still attenuate more or less these harmonic components. In the case of multi-harmonic excitation, Fig. 16(b) shows that all three components are effectively attenuated, especially for the 200 and 300 Hz. No noticeable amplification can be noted for other frequencies which are not directed related to the reference signal.

Feedback Controller was then tested. In this case, only single frequency disturbance case has been achieved. The result is presented in Fig. 17. It can be seen that the controller gives a 34.8 dB reduction after 6 s to control the first resonant frequency. More results are summarised in Table 4. The Feedback control algorithm is based on sensor feedback signals and is therefore more sensitive to the feedback noise, especially in the case where the coherence between the sensor and the actuator

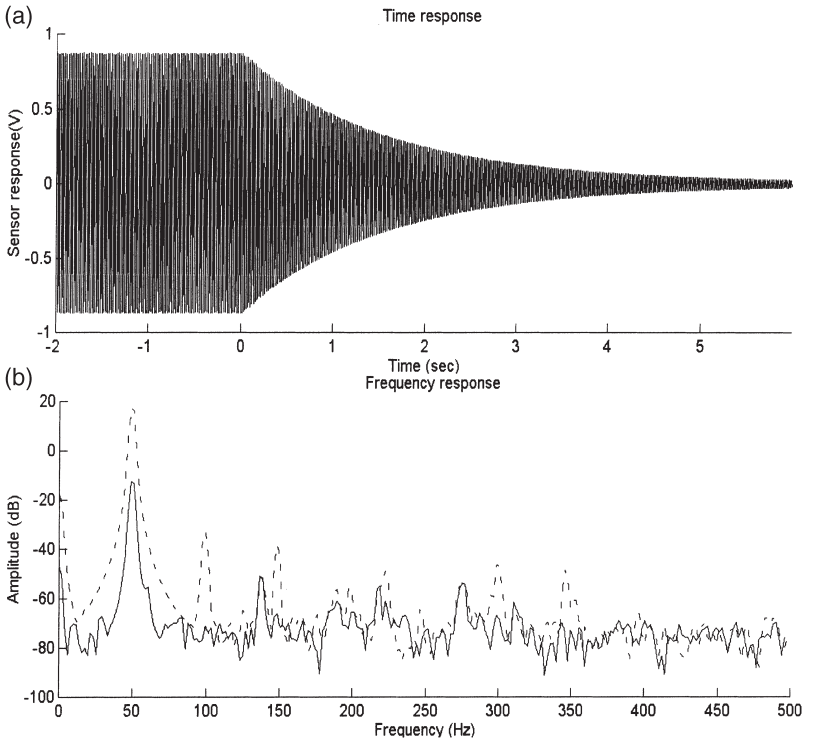

Fig. 15. Feedforward control of a single frequency signal (49.5 Hz) (a) time response (b) frequency response.

is poor. This is the case for 324 Hz which is a anti-resonance frequency for which the feedback signal is weak and therefore highly contaminated by noise.

Generally speaking, experimental results are consistent with simulated ones. Feedback control proved to be more difficult to achieve than feedforward control. In simulation however, no external noise was introduced so that good performance was achieved using feedback controller, which proved to be more or less true in experiments due to the noise contamination.

6. Conclusions

On the basis of a rectangular plate with symmetrically integrated piezo-elements, a semi-analytical model in time domain is presented in this paper. This model includes electromechanical effects of piezo-elements such as mass, stiffness and actuation. Some control simulation results are presented showing that the numerical model can be easily coupled with active control algorithms as a control simulator. Since the simulator includes every element involved in a real control process, the performance of the controller can be determined before its implementation. Experimental studies

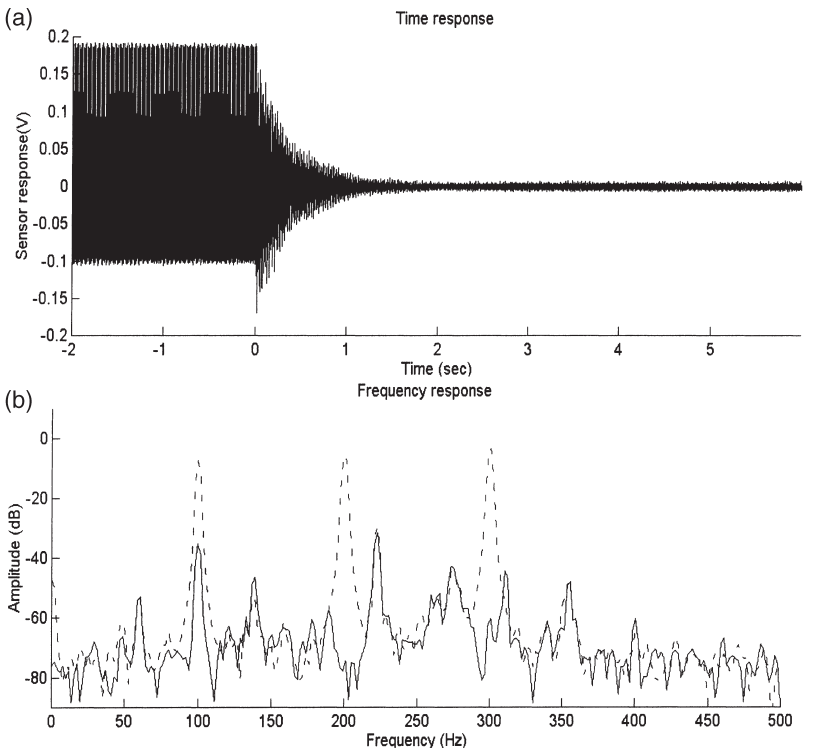

Fig. 16. Feedforward control of a multi-harmonic disturbance (100, 200 and 300 Hz) (a) time response; (b) frequency response.

using DSP are then performed and experimental results are presented. Experimental validation showed good agreement between the numerical model and the real system in the case of feedforward control. Improvement is still needed in the case of feedback control simulation due to the noise contamination. Generally speaking, it was observed that the model developed in this paper is accurate and flexible enough to represent the real system. The whole on-line simulation process is capable of reproducing reliable results to guide real-time implementation of controllers.

Acknowledgements

This work was supported by Structure R&D of Bombardier Aerospace in Toronto and NSERC. The authors would like particularly to thank Robby Lapointe and Barry Leigh for their collaboration. Also many thanks to Y. Jean, M. Gignac for making this work possible.

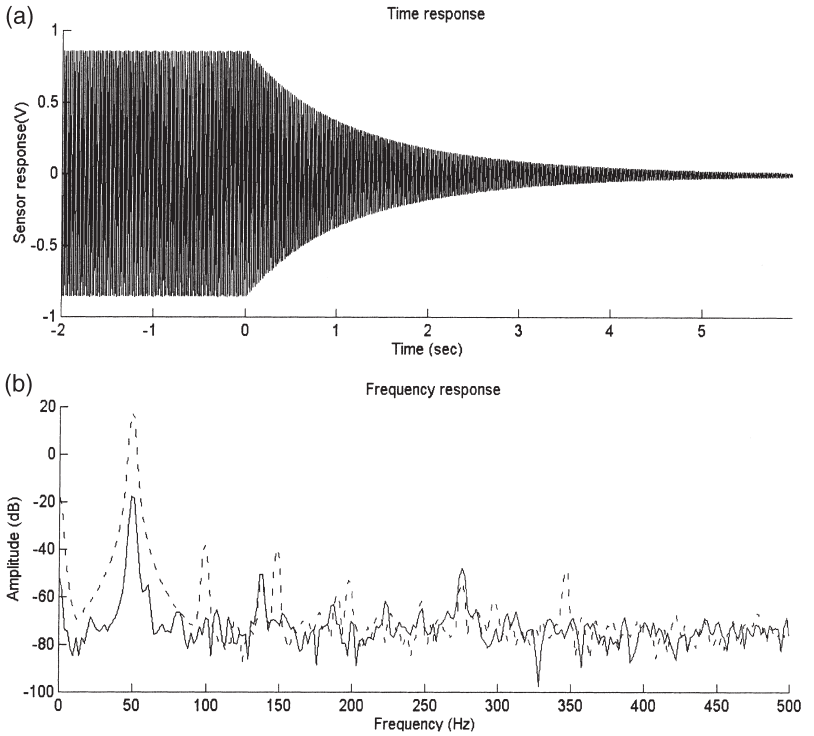

Fig. 17. Feedback control of a single frequency signal (49.5 Hz) (a) time response; (b) frequency response.

Table 4
Control performance for active control implementation

Feedforward control			Feedback Control		
Perturbation	Time (s)	Attenuation (dB)	Perturbation	Time (s)	Attenuation (dB)
Resonance (49.5 Hz)	6	29.8	Resonance (49.5 Hz)	6	34.8
Anti-resonance (170 Hz)	7	26.2	Anti-resonance (324 Hz)	N.A.[a]	N.A.
Non-resonance (100 Hz)	7	27.7	Non-resonance (100 Hz)	7	29.5
Multi-harmonic case (100, 200 and 300 Hz)	7	27.8	Multi-harmonic case (100, 200 and 300 Hz)	N.A.	N.A.

[a] N.A. Not achieved.

References

[1] Crawley EF, De Luis J. Use of piezoelectric actuators as elements of intelligent structures. AIAA J 1987;259:1373–85.

[2] Dimitriadis EK, Fuller CR, Rogers CA. Piezoelectric actuators for distributed vibration excitation of thin plates. Trans ASME, J Vib Acoust 1991;113:100–7.
[3] Gibbs GP, Fuller CR. Excitation of thin beams using asymmetric piezoelectric actuators. J Acoust Soc Am 1992;96:3221–7.
[4] Kim SJ, Jones JD. Influence of piezo-actuator thickness on the active vibration control of a cantilever beam. J Int Mat Syst Struct 1995;6:2047–53.
[5] Zhou S, Liang C, Rogers CA. An impedance-based system modeling approach for induced strain actuator-driven structures. Trans ASME, J Vib Acoust 1996;118:323–31.
[6] Proulx B, Cheng L. Dynamic modeling and analysis of plate vibration with integrated piezoceramic elements. Thin-wall Struct 2000;37:147–62.
[7] Jaffe B, Cook W, Jaffe H. Piezoelectric ceramics. London: Academic Press, 1971.
[8] Touzot G, Dhatt G. Une présentation de la méthode des éléments finis. Les presses de l'Université Laval, 1981.
[9] Widrow B, Stearns SD. Adaptive signal processing. Englewood Cliffs, NJ: Prentice-Hall, 1985.